Scalable Synthesis of TiO_2/Graphene Nanostructured Composite with High-Rate Performance for Lithium Ion Batteries

Xing Xin, Xufeng Zhou,* Jinghua Wu, Xiayin Yao, and Zhaoping Liu*

Ningbo Institute of Materials Technology and Engineering, Chinese Academy of Sciences Ningbo, Zhejiang 315201, P. R. China

ABSTRACT A simple and scalable method is developed to synthesize TiO_2/graphene nanostructured composites as high-performance anode materials for Li-ion batteries using hydroxyl titanium oxalate (HTO) as the intermediate for TiO_2. With assistance of a surfactant, amorphous HTO can condense as a flower-like nanostructure on graphene oxide (GO) sheets. By calcination, the HTO/GO nanocomposite can be converted to TiO_2/graphene nanocomposite with well preserved flower-like nanostructure. In the composite, TiO_2 nanoparticles with an ultrasmall size of several nanometers construct the porous flower-like nanostructure which strongly attached onto conductive graphene nanosheets. The TiO_2/graphene nanocomposite is able to deliver a capacity of 230 mA h g^{-1} at 0.1 C (corresponding to a current density of 17 mA g^{-1}), and demonstrates superior high-rate charge–discharge capability and cycling stability at charge/discharge rates up to 50 C in a half cell configuration. Full cell measurement using the TiO_2/graphene as the anode material and spinel $LiMnO_2$ as the cathode material exhibit good high-rate performance and cycling stability, indicating that the TiO_2/graphene nanocomposite has a practical application potential in advanced Li-ion batteries.

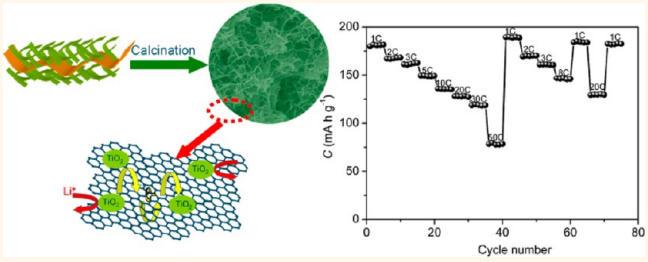

KEYWORDS: Li-ion battery · titania · graphene · anode · nanocomposite

With rising interest in green electrode materials for lithium-ion batteries (LIBs), increasing attention has been paid to titanium dioxide (TiO_2) anode material in recent years because of its long cycle life, low cost, and minimum environmental impact.[1,2] Moreover, the relatively high lithium insertion/extraction voltage of a TiO_2 anode (higher than 1.5 V *vs* Li^+/Li) can efficiently avoid the formation of SEI layers and lithium plating on the anode, which improves the safety of the batteries as compared with its carbon-based counterparts.[3–5] However, the practical application of the TiO_2 anode is still a challenge due to its low intrinsic electrical conductivity (10^{-12} S cm^{-1}) which leads to limited rate capability.[6–8]

The construction of TiO_2 nanostructures, for example, 1D nanowires or nanotubes,[9–13] 2D nanosheets,[14,15] and even complicated 3D structures with highly energetic facets as the dominant crystal face,[16–20] has been extensively studied in order to improve its rate performance by shortening the Li-ion and electron diffusion path, enlarging the electrode/electrolyte interfacial area as well as facilitating strain relaxation during the insertion/extraction processes.[21,22] However, the extremely low electrical conductivity of TiO_2 still limits its electrochemical performance. A combination of TiO_2 with conducting agents, such as metals,[23] metal oxides,[24,25] and carbonaceous materials[26] has proved to be an effective strategy to enhance electron transport. As compared with conventional conductive additives, the graphene nanosheet, as a new type of 2D carbon nanomaterial, appears particularly promising to improve the electrochemical performances of various electrode materials owing to its superior electrical conductivity, large surface area, and excellent structural flexibility.[27] Even at a very low weight fraction, graphene can serve as an efficient electron-conducting network and an excellent support that buffers the volume variation of electrode

* Address correspondence to liuzp@nimte.ac.cn, zhouxf@nimte.ac.cn.

Received for review October 11, 2012 and accepted November 26, 2012.

Published online November 26, 2012
10.1021/nn304725m

© 2012 American Chemical Society

materials.[28] Consequently, modification of TiO_2 anode material with graphene has attracted broad interest.

Direct hydrolysis of Ti(IV) precursors such as $TiCl_4$ and titanium alkoxide in aqueous solution is an easy process to produce TiO_2 nanostructures, which can also be employed to synthesize TiO_2/graphene nanocomposites.[29−31] However, Ti(IV) precursors have a very rapid hydrolysis rate, and even hydrolyzed instantly when exposed to moisture.[32] Accordingly, the as-prepared TiO_2 nanoparticles on graphene sheets usually have a relatively large particle size and/or are severely aggregated, which causes limited rate performance. Therefore, efforts have been made to address this problem by precisely controlling the formation process of TiO_2/graphene composites through various methods to obtain suitable nanostructures for fast electron and Li ion diffusion.[6,33−40] Yang *et al.* designed a TiO_2/graphene composite with sandwich-like structure using graphene and mesoporous silica as the template. Such TiO_2/graphene nanosheets with thickness of ∼50 nm provided numerous open channels for the access of electrolyte and facilitated the ultrafast diffusion of lithium ions during the cycling process. The composite could reach a high capacity of 80 mA h g^{-1} even at the high rate of 50 C.[6] Li *et al.* reported the synthesis of mesoporous TiO_2 nanospheres/graphene composite by a hydrothermal process. The rapid diffusion of electrolytes within the mesopores and electrons through thin TiO_2 walls, as well as highly conductive graphene sheets supporting TiO_2 spheres gave rise to excellent rate performance that a capacity of 97 mA h g^{-1} could be obtained when the discharge rate was as high as 50 C.[34] Ding *et al.* controlled the orientation of TiO_2 nanosheets loaded on graphene using solvothermal treatment to make sure that the (001) high-energy facets were exposed to electrolytes. The highly active facet endowed the composite with the capacity as high as 100 mA h g^{-1} at 20 C.[35] Other attempts to precisely control the particle size and nanostructure of TiO_2 on graphene nanosheets have also been reported using various methods, such as template-assisted synthsis,[36] an electrospun technique,[37] or hydrothermal treatment,[38−40] *etc.* Although the electrochemical performance of TiO_2/graphene composites can be remarkably improved in these cases, the synthetic routes, however, require relatively complicated experimental procedures and are not easy to be scaled up for practical application. Therefore, it is urgently desirable to develop a simple and cost-effective method for synthesizing TiO_2/graphene composites with optimized nanostructures as high performance anode materials.

In this paper, a simple and scalable method to synthesize high-performance TiO_2/graphene composite anode material *via* hydroxyl titanium oxalate (HTO, $Ti(OH)_2C_2O_4$) as the intermediate is presented. HTO with an amorphous nature has been studied as the coating layer in smart materials for electrorheological fluids, or as the precursor for preparing barium titanate.[41,42] No attempt of using HTO as the precursor to TiO_2 for energy storage applications has been carried out to the best of our knowledge. HTO can be easily synthesized through the reaction

$$Ti(OC_4H_9)_4 + H_2C_2O_4 + 2H_2O \rightarrow Ti(OH)_2C_2O_4\downarrow + 4C_4H_9OH$$

Further calcination can convert HTO to TiO_2 with controllable polymorphs. Compared with the fast hydrolysis process of tetrabutyl titanate (TBT) in water, the reaction between TBT and oxalic acid (OA) to form HTO is much less vigorous and proceeds gradually in a much longer time span (tens of minutes). Consequently, the structure and morphology of HTO can be easily tuned using simple and existing solution chemistry techniques; hence TiO_2 anode materials with desirable nanostructures can be obtained. In our experiments, HTO with a unique flower-like architecture attached to graphene oxide (GO) sheets was synthesized in the GO solution containing sodium dodecyl benzene sulfonate (SDBS) as the surfactant under mild reaction conditions. By calcination, this intermediate can be successfully converted into TiO_2/graphene nanocomposite which still remains the flower-like nanostructure. The final product exhibits outstanding rate capability due to its novel structure that facilitates fast diffusion of lithium ions and electrons during charge/discharge processes. Moreover, the simple and low-cost HTO mediated synthetic process can be easily scaled up. A scale of 1 kg/batch was successfully realized in our lab. Further verification of the electrochemical performance of as-prepared TiO_2/graphene composite by commercial full cells with a capacity of ∼1 Ah shows its great potential as a high-rate anode material for advanced LIBs.

RESULTS AND DISCUSSION

The synthesis strategy for different TiO_2-based samples is schematically depicted in Scheme 1. OA can remarkably reduce the hydrolysis rate of TBT, and the reaction between TBT and OA generates an amorphous HTO complex (refer to Figure S1, Supporting Information). As observed in our experiments, the white precipitate of HTO started to form 10 min after the dropwise addition of TBT, and the reaction proceeded gradually during the whole time range (∼40 min) of the addition of TBT. Therefore, it is easy to control the reaction process, and consequently the structure and morphology of HTO products by using suitable additives, due to the slow reaction rate. The morphologies of HTO are strongly affected by the additives, as shown in Figure 1. Without adding SDBS, the HTO sample shows an irregular particulate morphology under SEM characterization (Figure 1a). This product is named *p*-HTO hereafter. The TEM image (Figure 1b) reveals that the particles of *p*-HTO have sizes ranging from

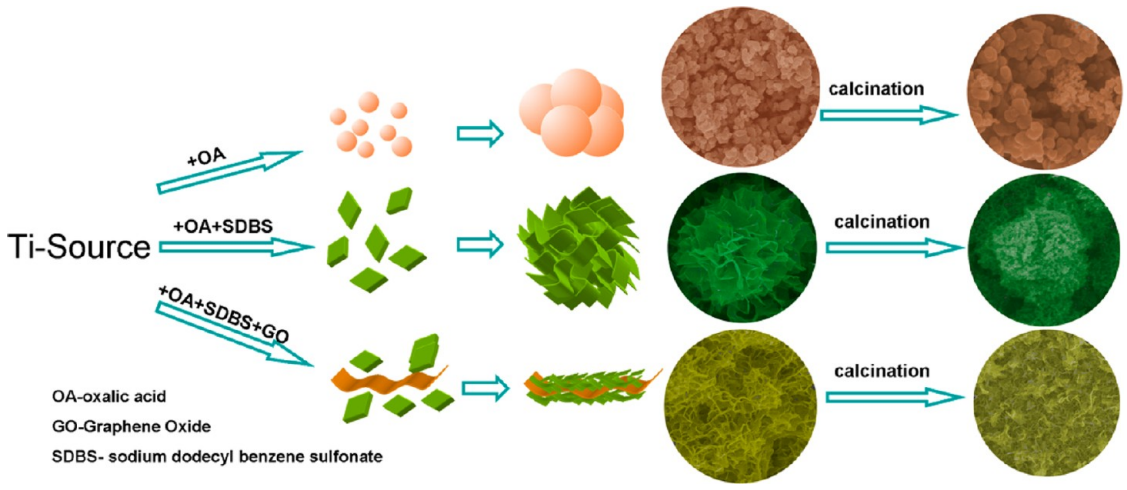

Scheme 1. Illustration of the preparation processes and growth mechanisms of TiO_2-based nanocomposites.

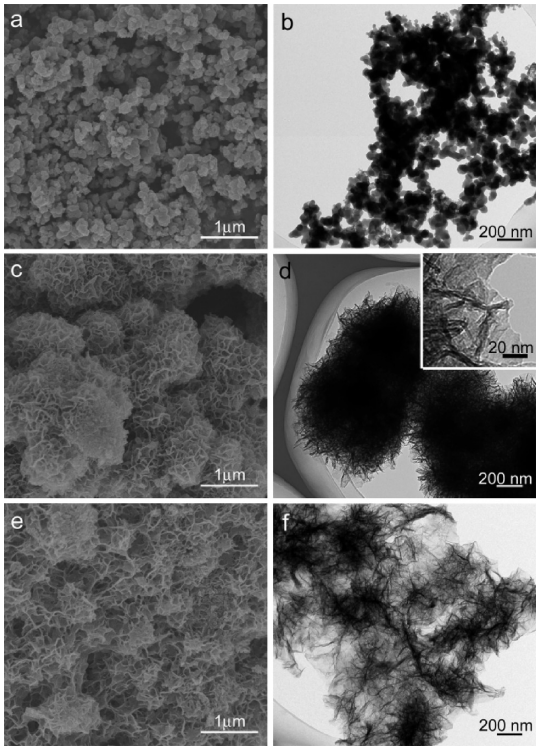

Figure 1. SEM and TEM images of *p*-HTO (a, b), *f*-HTO (c, d), and *f*-HTO/GO (e, f).

30 to 40 nm, and they aggregate severely. The morphology of HTO changes when SDBS is added, as shown in Figure 1c. The product (named *f*-HTO hereafter) consists of flower-like particles with diameters of *ca.* 1–1.5 μm. The detailed structural characterization by TEM (Figure 1d) reveals that the entire flower-like nanostructure is composed of intercrossed nanosheets which are 5–10 nm thick, and connected to each other to form a complicated 3D structure. When the morphologies of *p*-HTO and *f*-HTO are compared, it can be concluded that SDBS plays an important role in HTO growth. As an anionic surfactant, SDBS can significantly change the interface property between hydrophobic TBT and water, and thus affects the hydrolysis process of TBT, which alters the morphology of HTO from isotropic nanoparticles to anisotropic sheet-like nanostructures. When GO sheets are further introduced with a weight ratio of GO/TBT = 2/50, HTO nanosheets can grow uniformly on both sides of the GO sheets as shown in Figure 1e and f. Hereafter, this product is named *f*-HTO/GO. As compared with *f*-HTO in which nanosheets are interconnected to form relatively dense aggregates, in *f*-HTO/GO, HTO nanosheets are loosely distributed on GO due to the large surface area of GO sheets. It is also noted that HTO does not separate from GO sheets even under ultrasonication treatment, indicating that HTO and GO are strongly bonded rather than loosely aggregated.

To understand the formation process of *f*-HTO/GO, the structures of intermediate products sampled every 5 min during the addition of TBT are characterized as shown in Figure S2 (Supporting Information). Tiny nanoparticles with diameters smaller than 10 nm can be found on the GO sheets after 10 min of TBT addition, and both of the amounts and the size of HTO increase along with the reaction time. It is interesting that nanoparticles rather than nanosheets are observed during 15–25 min, and a mixture of nanosheets and nanoparticles are discerned at 30 min. After 35 min, pure nanosheets are formed finally. The effect of GO on the structure of HTO is also investigated by varying the ratio of GO/TBT as shown in Figure S3 (Supporting Information). It is found that at a low weight ratio of 1/50, HTO attached to the surface of GO is obviously aggregated. When the GO content is increased, the density of HTO on the GO sheets gradually decreases, and its extent of aggregation also declines. When the weight ratio of GO is higher than 2.5/50, some bare GO surface can be observed. Therefore, the weight ratio of GO/TBT = 2/50 is proper in our experiments to achieve uniform and loose distribution of HTO on GO sheets.

Thermal decomposition can easily transform HTO into TiO_2. The polymorphs of TiO_2 strongly depend on

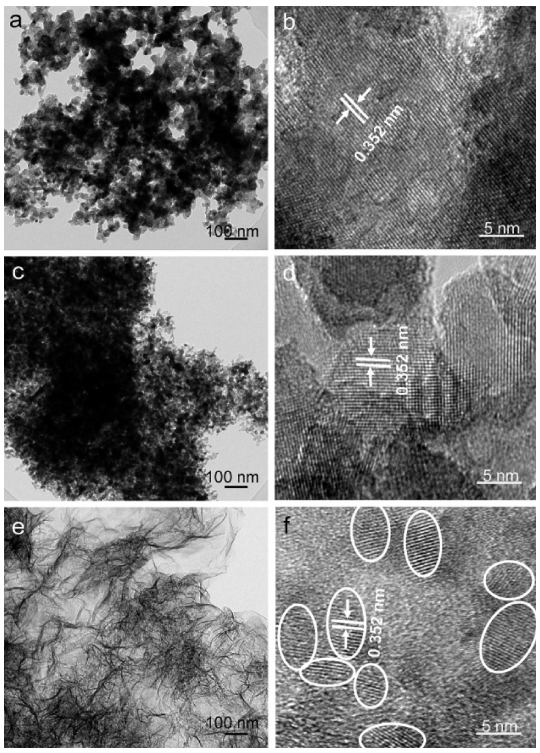

Figure 2. TEM and HRTEM images of *p*-TiO_2 (a, b), *f*-TiO_2 (c, d) and *f*-TiO_2/G (e, f).

the calcination temperature. Previous researches have revealed that the anatase phase exhibits a better electrochemical performance than the rutile one.[2,14] Consequently, the calcination process in our experiments was carried out at 450 °C to ensure the formation of pure anatase, which can be proved by the XRD results (Figure S4, Supporting Information). After calcination, the *p*-HTO decomposes to *p*-TiO_2 which still possesses the particulate morphology with a mean diameter of 20−30 nm as shown in Figure 2a,b and Figure S5a (Supporting Information). However, the products aggregate severely due to the fusion of nanoparticles during thermal treatment. For *f*-HTO, calcination destroys the characteristic flower-like morphology, and aggregations of TiO_2 nanoparticles are gained (Figure 2c,d and Figure S5b, Supporting Information) in the product of *f*-TiO_2. High resolution TEM characterization reveals that TiO_2 nanoparticles have diameters of 10−20 nm. The clearly visible set of lattice fringes with a period of 0.35 nm is characteristic of the (101) lattice planes of anatase TiO_2. For *f*-HTO/GO, after calcination, the resulted *f*-TiO_2/G composite retains almost identical morphology, as observed in the TEM image with a low magnification (Figure 2e). Flower-like TiO_2 nanosheets distribute homogeneously on thermally reduced graphene sheets. A high resolution TEM image (Figure 2f) further shows that the walls of the TiO_2 nanosheets are composed of tiny TiO_2 nanoparticles whose diameters are in the range of 5−10 nm, which are apparently smaller than those in

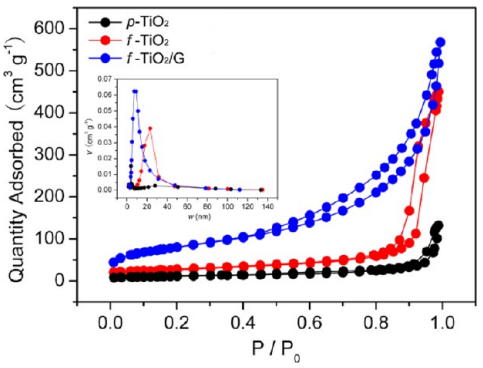

Figure 3. Nitrogen adsorption−desorption isotherms of *p*-TiO_2, *f*-TiO_2, and *f*-TiO_2/G. The inset shows their pore-size distribution plots.

the sample of *f*-TiO_2. The lattice fringes observed in *f*-TiO_2/G are also consistent with the (101) lattice plane of anatase.

The specific surface area and pore size distribution of three TiO_2 samples are further investigated by nitrogen adsorption−desorption measurement, and their isotherms are shown in Figure 3. The specific surface area of *f*-TiO_2 is calculated to be 92.6 $m^2\ g^{-1}$, much higher than that of *p*-TiO_2 (38.8 $m^2\ g^{-1}$), which can be ascribed to the smaller particle size of the former sample. *f*-TiO_2/G possesses an even higher specific surface area of 211.6 $m^2\ g^{-1}$, which should be mainly attributed to the contribution of graphene, as well as the smaller crystal size of TiO_2 nanoparticles in *f*-TiO_2/G. The pore size distribution plots calculated from the desorption isotherm using the Barrett−Joyner−Halenda (BJH) method (inset image in Figure 3) indicates the presence of rather uniform mesopores with an average pore diameter of 22 nm in *f*-TiO_2 and 10 nm in *f*-TiO_2/G. On the basis of the electron microscopy data, such mesopores in both samples are ascribed to the interparticle space caused by the random stacking of TiO_2 nanoparticles. Therefore, the smaller pore diameters in *f*-TiO_2/G reflect its smaller particle sizes, coincident with the results from SEM and TEM characterization.

The electrochemical performance of *p*-TiO_2, *f*-TiO_2, and *f*-TiO_2/G as anode materials is comprehensively evaluated in lithium half-cells. Figure 4a presents the first galvanostatic discharging/charging curves of three samples at 0.1 C within a cutoff window of 1.0−3.0 V. All three materials display a discharge voltage plateau at 1.78 ± 0.01 V and a charge voltage plateau at 1.98 ± 0.01 V, which are characteristic of anatase TiO_2. The initial discharge and charge capacities of three samples are all above 200 mA h g^{-1}, which are higher than the theoretical capacity of bulk titania (167.5 mA h g^{-1}) with the maximum lithium insertion coefficient of 0.5 ($Li_{0.5}TiO_2$) based on the following electrochemical reaction: $TiO_2 + xLi + xe^- \leftrightarrow Li_xTiO_2$ ($0 \le x \le 0.5$).[43,44] Among three titania samples, *f*-TiO_2/G shows the highest discharge and charge capacity of 280 and 226 mA h g^{-1},

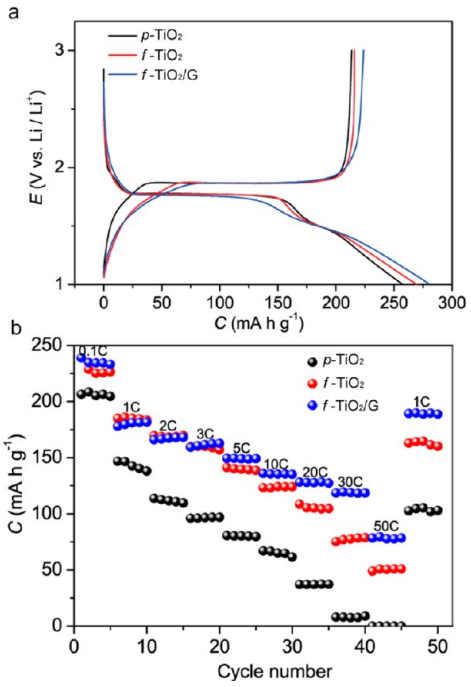

Figure 4. (a) Curves for galvanostatic discharge/charge of TiO_2 at 0.1 C. (b) Rate capability of *p*-TiO_2, *f*-TiO_2, and *f*-TiO_2/G. The Li^+ insertion rate (discharge) and Li^+ extraction (charge) rate were changed from 0.1 to 50 C.

respectively, *f*-TiO_2 shows intermediate, and *p*-TiO_2 shows the lowest, which might be attributed to the difference of the particle size and structure in these anode materials. *f*-TiO_2/G which is modified by graphene and possesses the smallest particle size among three samples is believed to have the best ionic and electronic conductivity. It is noticed that *f*-TiO_2/G has a shorter voltage plateau and longer terminal voltage slope in its discharge curve as compared with the other two samples. The voltage slope is generally considered as capacitive behavior of the surface or interfacial storage of lithium ions, whose proportion in the total discharge capacitance increases when the particle size decreases.[45−47] Such phenomenon can be observed in other nanostructured materials, such as $LiFePO_4$[48] and $LiMn_2O_4$.[49] It should be mentioned here that graphene is also electrochemically active within the current voltage window as reported earlier.[50,51] It normally has a reversible capacity higher than 500 mA h g^{-1}, and typical slope-like charge or discharge curves with no plateau. Subsequently, the existence of graphene in *f*-TiO_2/G may contribute partially in its relatively higher capacity and longer voltage slope in the discharge/charge curves as compared with those of *f*-TiO_2.

Figure 4b presents the rate capability of three anode materials tested from 0.1 to 50 C with identical discharge and charge current density and five discharge/charge cycles at each rate. The results show that in the initial several cycles at a low rate of 0.1 C, both *f*-TiO_2 and *f*-TiO_2/G possess a distinctly higher capacity than *p*-TiO_2. At higher rates from 1 to 3 C, the capacities of *f*-TiO_2 and *f*-TiO_2/G are comparable. Both have a capacity retention rate of 70% at the rate of 3 C. The capacity of *p*-TiO_2, however, fades quickly when the rate increases, whose retention rate at 3 C is smaller than 50%. The capacities of *f*-TiO_2 and *f*-TiO_2/G tend to differentiate above the rate of 5 C. The capacity of *f*-TiO_2/G apparently exceeds that of *f*-TiO_2 when the rate is raised to 10 C, and their difference gradually becomes larger along with the increase of the rate. At the high rate of 50 C, *f*-TiO_2/G reaches a capacity of 80 mA h g^{-1} (35% of the initial capacity), which is ~30% higher than that of *f*-TiO_2 (60 mA h g^{-1}). After the high rate test, the cells are remeasured at a relatively low rate of 1 C again. It is surprising to find that the remeasured capacity for *f*-TiO_2/G even exceeds the one measured during the initial 1 C cycles. The same phenomenon has been observed in some earlier reports,[6,20] which may be ascribed to the activation process of the electrode materials during cycling. However, the remeasured capacity for *f*-TiO_2 and *p*-TiO_2 are only 95% and 83% of their initial ones, respectively. Consequently, *f*-TiO_2/G possesses superior rate capability than *f*-TiO_2 and *p*-TiO_2. Cyclic voltammograms (CVs) of *f*-TiO_2/G at different scan rates (0.2−5.0 mV s^{-1}) are shown in Figure S6 (Supporting Information). A pair of redox peaks can be clearly observed even at a scan rate of 5 mV s^{-1}. These peaks correspond to the reversible biphasic transition between tetragonal anatase and orthorhombic Li_xTiO_2.[52] The good symmetry of the redox peaks at all scan rates further suggests the outstanding rate capability of *f*-TiO_2/G. The effect of graphene content (measured by TGA as shown in Figure S5h, Supporting Information) in the *f*-TiO_2/G sample is also evaluated. It is found in Figure S7 (Supporting Information) that samples with 8 wt % of graphene (corresponding to the weight ratio of GO/TBT = 2/50) exhibit the best electrochemical performance. Lower graphene content leads to poor rate capability probably due to relatively severe aggregation of TiO_2 (Figure S5c, Supporting Information), while higher graphene content results in lower capacity because of less weight fraction of active titania materials.

The *f*-TiO_2/G also demonstrates excellent cycling stability at high current densities. Lithium cells using *f*-TiO_2/G as the cathode were run at constant rates of 1, 10, 20 C, respectively, after being aged at 0.1 C for 2 cycles. Approximately 97%, 98%, and 99% of its initial charge capacity is retained after 100 discharge/charge cycles at 1, 10, and 20 C, respectively as shown in Figure 5a. The average capacity fading per cycle is as small as 0.03%, and the Coulombic efficiency is nearly 100% at each cycle. The cycling stability of *f*-TiO_2/G is also measured at randomly varied rates within the range of 1−50 C. Figure 5b shows that a large capacity of nearly 180 mA h g^{-1}, which is comparable to the initial capacity in the first cycle, was achieved when the current rate was returned to 1 C even after 70 cycles at high current rates up to 50 C. Such outstanding rate

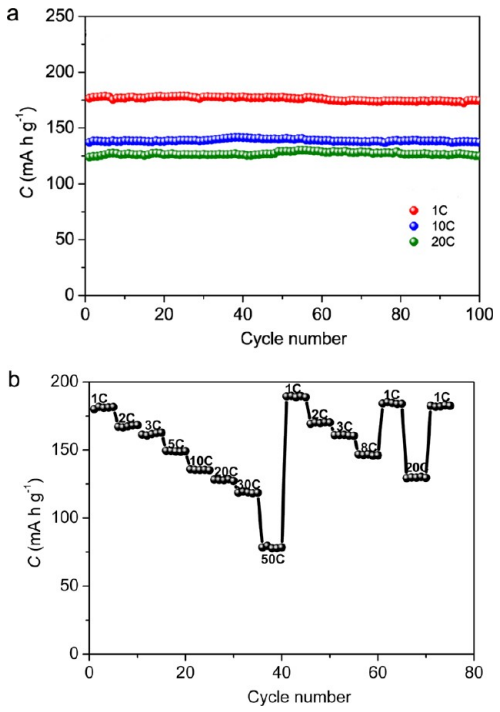

Figure 5. (a) Li^+ extraction capacity *vs* cycle number of *f*-TiO_2/G nanocomposite; (b) typical cycling behavior of *f*-TiO_2/G coin-type cells at various rates of discharge.

capability and cycling stability excel reported titania materials and make *f*-TiO_2/G a good candidate for anode materials in high power lithium batteries.[3,24,29−31] The outstanding electrochemical performance can be attributed to the unique nanostructure of *f*-TiO_2/G. On one hand, the ultrasmall particle size of *f*-TiO_2/G not only guarantees the shorter Li^+ diffusion length which is the key to improve the rate performance, but also enhances the storage capacity which is the main characteristic of the nanostructured electrode material. On the other hand, the existence of graphene as a conducting agent greatly improves the electrical conductivity of the nanocomposite. In addition, graphene sheets with a large surface area also serve as substrates that effectively inhibit the aggregation of titania nanoparticles, which remarkably raises the homogeneity of the Li ion insertion/extraction. More importantly, as compared with those of previous reports, the synthetic route for *f*-TiO_2/G provided in this paper is easier to operate and nontoxic, therefore can be readily scaled up. A scale of 1 kg/batch was conveniently realized in our lab, which shows the attractive application potential of *f*-TiO_2/G anode materials in commercial lithium ion batteries.

To evaluate the practical performance of *f*-TiO_2/G in commercial batteries, a prototype of 18650-type full cell was manufactured by using *f*-TiO_2/G as the anode active material, and spinel $LiMn_2O_4$ as the cathode active material. The voltage profile of the full cell is shown in Figure 6a. It discharges at an average voltage of 2.1 V, lower than commercial $LiMn_2O_4$ cells, due to the relatively higher charge potential of titania than

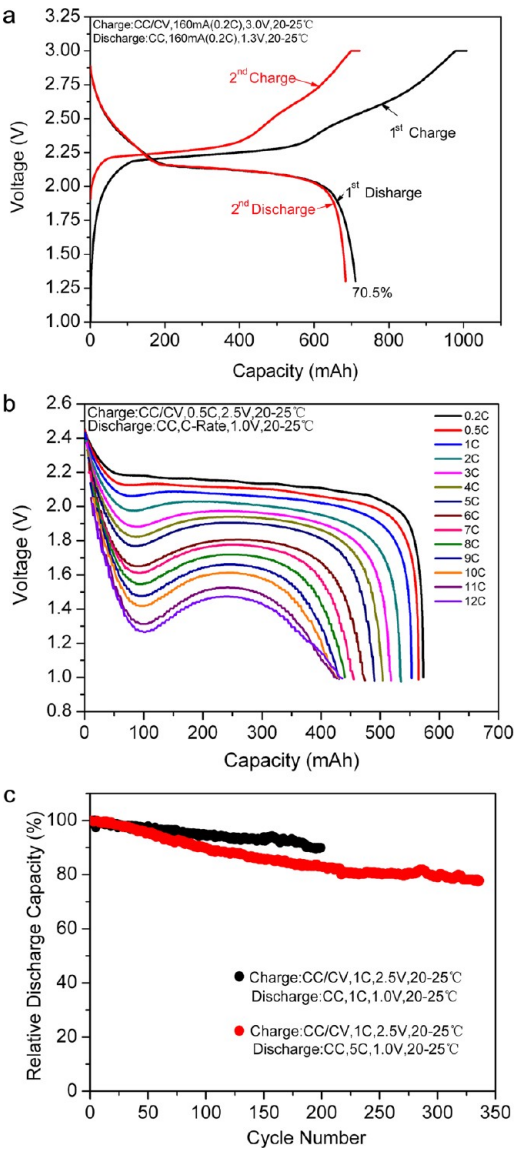

Figure 6. (a) Curves for galvanostatic discharge/charge of $LiMn_2O_4$-*f*-TiO_2/G full cell at 0.2C; (b) curves for galvanostatic discharge/charge of the full cell at different rates; (c) discharge capacity *vs* cycle number of the full cell. The charge rate was fixed at 1 C while the discharge rates were 1 and 5 C.

commercial graphite anode materials. The cell delivers an initial discharge capacity of 700 mA h which is close to the designed capacity of 800 mA h. The rate capability and cycling performance are demonstrated in Figure 6b,c. The discharge capacity slowly decays along with the increase of the current rate. When the discharge current is as high as 12 C, the cell still reaches a discharge capacity of ~430 mA h, approximately 60% of its capacity at 0.2 C. The full cell has a capacity retention rate of 90% after 200 cycles under a 1 C charge/discharge rate, and 80% after 300 cycles under a 5 C rate, which is comparable or even better than commercial $LiMn_2O_4$ batteries using graphite anode. However, the large surface area of *f*-TiO_2/G gives rise to a relatively large initial irreversible capacity (Figure 6a)

and a low compact density. Therefore, the synthesis of *f*-TiO_2/G needs further optimization to pave the way to the practical applications of this new type of anode materials in lithium ion batteries.

CONCLUSIONS

An environmental benign and high yield method has been developed for the synthesis of TiO_2/graphene nanocomposites as anode materials for LIBs. Using HTO as the precursor to TiO_2, the hydrolysis of titanium alkoxides can be easily controlled, and a unique architecture that ultrasmall anatase nanoparticles assembled in a flower-like structure and strongly bonded to the surface of graphene sheets can be successfully obtained. The nanosized TiO_2 particles, porous structure and highly conductive graphene provide negligible diffusion time, fast phase transfer reaction and enhanced local conductivity, resulting in exceptionally high rate capability and excellent cycling stability. The synthesis route provided in this paper only requires mild reagents and ambient reaction conditions, which is anticipated to be a scalable production method for high performance TiO_2-based anode materials to be used in the next-generation LIBs.

EXPERIMENTAL METHODS

Material Synthesis. Graphene oxide (GO) nanosheets were prepared according to the method we reported previously.[53] The experiment details are described in the Supporting Information. In a typical synthesis, 30 mL of ethanol solution containing 5 g of $Ti(OC_4H_9)_4$ (tetrabutyl titanate, TBT) and 0.3 g of acetic acid was dropwise added into 60 mL of water/ethanol solution (3:1, in volume) containing 2 g of oxalic acid (OA), 0.2 g of SDBS, and 0.2 g of graphene oxide (GO) nanosheets under stirring at 50 °C. The resulting light brown slurry was further stirred for 3 h and additionally aged for 1 h. The precipitate was collected by centrifuge and repeatedly washed with ethanol and deionized water, and then air-dried at 80 °C. The obtained nanocomposite was further calcinated at 450 °C for 5 h, resulting in the final product. The weight ratio of GO/TBT was tuned to 1/50, 1.5/50, 2/50, 2.5/50, and 3/50, respectively, in our experiments. The corresponding weight content of graphene in the final products is measured to be 4, 6, 8, 10, and 12 wt %, respectively, using thermal gravimetric analysis. For comparison, the samples synthesized without adding GO and/or SDBS were also prepared using the same synthesis procedures.

Structural Characterizations. Powder X-ray diffraction (XRD) measurements were performed using an AXS D8 Advance diffractometer (Cu Kα radiation; receiving slit, 0.2 mm; scintillation counter, 40 mA; 40 kV) from Bruker Inc. The morphology and structure were analyzed by a Hitachi S-4800 field emission scanning-electron microscope (SEM) and an FEI Tecnai G^2 F20 transmission-electron microscope (TEM) at an accelerating voltage of 200 kV. The nitrogen sorption isotherms (BET) were recorded by a Micromeritics ASAP-2020 M nitrogen adsorption apparatus. Pore size distribution plot was obtained by the Barrett–Joyner–Halenda (BJH) method. Thermal gravimetric analysis (TGA) was performed on a Pyris Diamond thermogravimetric/differential thermal analyzer by Perkin-Elmer.

Electrochemical Tests. The evaluation of electrochemical performance was carried out in both CR2032-type coin cells and 18650-type full cells. For the coin cells, the working electrode contained 80 wt % of active materials, 10 wt % of Super P, and 10 wt % of polyvinylidene fluoride (PVDF). The Li metal foil served as the counter electrode. The electrolyte was composed of 1 M $LiPF_6$ solution in ethylene carbonate (EC)/dimethyl carbonate (DMC) (1:1 by volume). The coin cells were activated at a current density of 0.1 C (17 mA g^{-1}) for the first cycle, and then cycled under different current densities within the voltage range of 1.0–3.0 V using a LAND-CT2001A battery test system (Jinnuo Wuhan Corp., China). For the full cells, the cathode contained 94 wt % of spinel $LiMn_2O_4$ as the active material, 3.8 wt % of Super P and 2.2 wt % of PVDF; the anode was composed of 93 wt % of TiO_2/graphene nanocomposite as the active material, 3.5 wt % of Super P and 3.5 wt % of PVDF. The full cells were activated at a current density of 0.1 C for the first three cycles, and then aged for about 3 days. Afterward, the cells were cycled under different current densities within the voltage range of 1.25–3 V.

Conflict of Interest: The authors declare no competing financial interest.

Supporting Information Available: Experimental details of GO preparation, additional XRD patterns, SEM images, TEM images, and electrochemical testing results of TiO_2/graphene nanocomposites. This material is available free of charge *via* the Internet at http://pubs.acs.org.

Acknowledgment. We are grateful for financial support from Zhejiang Provincial Natural Science Foundation of China (Grant No. R4100194), National Natural Science Foundation of China (Grant No. 21201173), the Key Research Program of the Chinese Academy of Sciences (Grant No. KGZD-EW-202-4), and the 973 program (Grant No. 2011CB935900). We thank Mr. Saixi Yaletu for synthesizing the $LiMn_2O_4$ cathode material and Mr. Huasheng Hu and Mr. Yongfeng Zeng for their helps in the fabrication and testing of the 18650-type full cells.

REFERENCES AND NOTES

1. Chen, X.; Mao, S. S. Titanium Dioxide Nanomaterials: Synthesis, Properties, Modifications, and Applications. *Chem. Rev.* **2007**, *107*, 2891–2959.
2. Deng, D.; Kim, M. G.; Lee, J. Y.; Cho, J. Green Energy Storage Materials: Nanostructured TiO_2 and Sn-based Anodes for Lithium-Ion Batteries. *Energy Environ. Sci.* **2009**, *2*, 818–837.
3. Han, H.; Song, T.; Bae, J.-Y.; Nazar, L. F.; Kim, H.; Paik, U. Nitridated TiO_2 Hollow Nanofibers as an Anode Material For High Power Lithium Ion Batteries. *Energy Environ. Sci.* **2011**, *4*, 4532–4536.
4. Zhang, J.; Yan, X.; Zhang, J.; Cai, W.; Wu, Z.; Zhang, Z. Preparation and Electrochemical Performance of TiO_2/C Composite Nanotubes as Anode Materials of Lithium-Ion Batteries. *J. Power Sources.* **2012**, *198*, 223–228.
5. Myung, S.-T.; Takahashi, N.; Komaba, S.; Yoon, C. S.; Sun, Y.-K.; Amine, K.; Yashiro, H. Nanostructured TiO_2 and Its Application in Lithium-Ion Storage. *Adv. Funct. Mater.* **2011**, *21*, 3231–3241.
6. Yang, S.; Feng, X.; Muellen, K. Sandwich-Like, Graphene-Based Titania Nanosheets with High Surface Area for Fast Lithium Storage. *Adv. Mater.* **2011**, *23*, 3575–3579.
7. Yang, Z.; Du, G.; Meng, Q.; Guo, Z.; Yu, X.; Chen, Z.; Guo, T.; Zeng, R. Synthesis of Uniform TiO_2@Carbon Composite Nanofibers as Anode for Lithium Ion Batteries with Enhanced Electrochemical Performance. *J. Mater. Chem.* **2012**, *22*, 5848–5854.
8. Moriguchi, I.; Hidaka, R.; Yamada, H.; Kudo, T.; Murakami, H.; Nakashima, N. A Mesoporous Nanocomposite of TiO_2 and Carbon Nanotubes as a High-Rate Li-Intercalation Electrode Material. *Adv. Mater.* **2006**, *18*, 69–73.
9. Han, H.; Song, T.; Lee, E.-K.; Devadoss, A.; Jeon, Y.; Ha, J.; Chung, Y.-C.; Choi, Y.-M.; Jung, Y.-G.; Paik, U. Dominant Factors Governing the Rate Capability of a TiO_2 Nanotube Anode for High Power Lithium Ion Batteries. *ACS Nano* **2012**, *6*, 8308–8315.

10. Wang, K.; Wei, M.; Morris, M. A.; Zhou, H.; Holmes, J. D. Mesoporous Titania Nanotubes: Their Preparation and Application as Electrode Materials for Rechargeable Lithium Batteries. *Adv. Mater.* **2007**, *19*, 3016–3020.
11. Luo, W.; Hu, X.; Sun, Y.; Huang, Y. Surface Modification of Electrospun TiO_2 Nanofibers *via* Layer-by-Layer Self-Assembly for High-Performance Lithium-Ion Batteries. *J. Mater. Chem.* **2012**, *22*, 4910–4915.
12. Brutti, S.; Gentili, V.; Menard, H.; Scrosati, B.; Bruce, P. G. TiO_2-(B) Nanotubes as Anodes for Lithium Batteries: Origin and Mitigation of Irreversible Capacity. *Adv. Energy Mater.* **2012**, *2*, 322–327.
13. Das, S. K.; Bhattacharyya, A. J. High Lithium Storage in Mixed Crystallographic Phase Nanotubes of Titania and Carbon–Titania. *J. Phys. Chem. C* **2009**, *113*, 17367–17371.
14. Chen, J. S.; Lou, X. W. Anatase TiO_2 Nanosheet: An Ideal Host Structure for Fast and Efficient Lithium Insertion/Extraction. *Electrochem. Commun.* **2009**, *11*, 2332–2335.
15. Liu, J.; Chen, J. S.; Wei, X.; Lou, X. W.; Liu, X.-W. Sandwich-like, Stacked Ultrathin Titanate Nanosheets for Ultrafast Lithium Storage. *Adv. Mater.* **2011**, *23*, 998–1002.
16. Yang, H. G.; Sun, C. H.; Qiao, S. Z.; Zou, J.; Liu, G.; Smith, S. C.; Cheng, H. M.; Lu, G. Q. Anatase TiO_2 Single Crystals with a Large Percentage of Reactive Facets. *Nature* **2008**, *453*, 638–642.
17. Chen, J. S.; Tan, Y. L.; Li, C. M.; Cheah, Y. L.; Luan, D.; Madhavi, S.; Boey, F. Y. C.; Archer, L. A.; Lou, X. W. Constructing Hierarchical Spheres from Large Ultrathin Anatase TiO_2 Nanosheets with Nearly 100% Exposed (001) Facets for Fast Reversible Lithium Storage. *J. Am. Chem. Soc.* **2010**, *132*, 6124–6130.
18. Liu, S.; Yu, J.; Jaroniec, M. Anatase TiO_2 with Dominant High-Energy {001} Facets: Synthesis, Properties, and Applications. *Chem. Mater.* **2011**, *23*, 4085–4093.
19. Ye, J.; Liu, W.; Cai, J.; Chen, S.; Zhao, X.; Zhou, H.; Qi, L. Nanoporous Anatase TiO_2 Mesocrystals: Additive-Free Synthesis, Remarkable Crystalline-Phase Stability, and Improved Lithium Insertion Behavior. *J. Am. Chem. Soc.* **2011**, *133*, 933–940.
20. Hong, Z.; Wei, M.; Lan, T.; Jiang, L.; Cao, G. Additive-Free Synthesis of Unique TiO_2 Mesocrystals with Enhanced Lithium-Ion Intercalation Properties. *Energy Environ. Sci.* **2012**, *5*, 5408–5413.
21. Hu, Y. S.; Kienle, L.; Guo, Y. G.; Maier, J. High Lithium Electroactivity of Nanometer-Sized Rutile TiO_2. *Adv. Mater.* **2006**, *18*, 1421–1426.
22. Bruce, P. G.; Scrosati, B.; Tarascon, J.-M. Nanomaterials for Rechargeable Lithium Batteries. *Angew. Chem., Int. Ed.* **2008**, *47*, 2930–2946.
23. Wang, W.; Tian, M.; Abdulagatov, A.; George, S. M.; Lee, Y.-C.; Yang, R. Three-Dimensional Ni/TiO_2 Nanowire Network for High Areal Capacity Lithium Ion Microbattery Applications. *Nano Lett.* **2012**, *12*, 655–660.
24. Luo, Y.; Luo, J.; Jiang, J.; Zhou, W.; Yang, H.; Qi, X.; Zhang, H.; Fan, H. J.; Yu, D. Y. W.; Li, C. M.; *et al.* Seed-Assisted Synthesis of Highly Ordered TiO_2@alpha-Fe_2O_3 Core/Shell Arrays on Carbon Textiles for Lithium-Ion Battery Applications. *Energy Environ. Sci.* **2012**, *5*, 6559–6566.
25. Park, K.-S.; Kang, J.-G.; Choi, Y.-J.; Lee, S.; Kim, D.-W.; Park, J.-G. Long-Term, High-Rate Lithium Storage Capabilities of TiO_2 Nanostructured Electrodes Using 3D Self-Supported Indium Tin Oxide Conducting Nanowire Arrays. *Energy Environ. Sci.* **2011**, *4*, 1796–1801.
26. Guo, Y.-G.; Hu, Y.-S.; Sigle, W.; Maier, J. Superior Electrode Performance of Nanostructured Mesoporous TiO_2 (Anatase) through Efficient Hierarchical Mixed Conducting Networks. *Adv. Mater.* **2007**, *19*, 2087–2091.
27. Kamat, P. V. Graphene-Based Nanoassemblies for Energy Conversion. *J. Phys. Chem. Lett.* **2011**, *2*, 242–251.
28. Liang, M.; Zhi, L. Graphene-Based Electrode Materials for Rechargeable Lithium Batteries. *J. Mater. Chem.* **2009**, *19*, 5871–5878.
29. Lambert, T. N.; Chavez, C. A.; Hernandez-Sanchez, B.; Lu, P.; Bell, N. S.; Ambrosini, A.; Friedman, T.; Boyle, T. J.; Wheeler, D. R.; Huber, D. L. Synthesis and Characterization of Titania-Graphene Nanocomposites. *J. Phys. Chem. C* **2009**, *113*, 19812–19823.
30. Tao, H.-C.; Fan, L.-Z.; Yan, X.; Qu, X. *In Situ* Synthesis of TiO_2–Graphene Nanosheets Composites as Anode Materials for High-Power Lithium Ion Batteries. *Electrochim. Acta* **2012**, *69*, 328–333.
31. Shen, L.; Zhang, X.; Li, H.; Yuan, C.; Cao, G. Design and Tailoring of a Three-Dimensional TiO_2-Graphene–Carbon Nanotube Nanocomposite for Fast Lithium Storage. *J. Phys. Chem. Lett.* **2012**, *2*, 3096–3101.
32. Sun, Z.; Kim, J. H.; Zhao, Y.; Bijarbooneh, F.; Malgras, V.; Lee, Y.; Kang, Y.-M.; Dou, S. X. Rational Design of 3D Dendritic TiO_2 Nanostructures with Favorable Architectures. *J. Am. Chem. Soc.* **2011**, *133*, 19314–19317.
33. Wang, D.; Choi, D.; Li, J.; Yang, Z.; Nie, Z.; Kou, R.; Hu, D.; Wang, C.; Saraf, L. V.; Zhang, J.; *et al.* Self-Assembled TiO_2–Graphene Hybrid Nanostructures for Enhanced Li-Ion Insertion. *ACS Nano* **2009**, *3*, 907–914.
34. Li, N.; Liu, G.; Zhen, C.; Li, F.; Zhang, L.; Cheng, H.-M. Battery Performance and Photocatalytic Activity of Mesoporous Anatase TiO_2 Nanospheres/Graphene Composites by Template-Free Self-Assembly. *Adv. Funct. Mater.* **2011**, *21*, 1717–1722.
35. Ding, S.; Chen, J. S.; Luan, D.; Boey, F. Y. C.; Madhavi, S.; Lou, X. W. Graphene-Supported Anatase TiO_2 Nanosheets for Fast Lithium Storage. *Chem. Commun.* **2011**, *47*, 5780–5782.
36. Chen, J. S.; Wang, Z.; Dong, X. C.; Chen, P.; Lou, X. W. Graphene-Wrapped TiO_2 Hollow Structures with Enhanced Lithium Storage Capabilities. *Nanoscale* **2011**, *3*, 2158–2161.
37. Zhang, X.; Kumar, P. S.; Aravindan, V.; Liu, H. H.; Sundaramurthy, J.; Mhaisalkar, S. G.; Duong, H. M.; Ramakrishna, S.; Madhavi, S. Electrospun TiO_2–Graphene Composite Nanofibers as a Highly Durable Insertion Anode for Lithium Ion Batteries. *J. Phys. Chem. C* **2012**, *116*, 14780–14788.
38. Cai, D.; Lian, P.; Zhu, X.; Liang, S.; Yang, W.; Wang, H. High Specific Capacity of TiO_2–Graphene Nanocomposite as an Anode Material for Lithium-Ion Batteries in an Enlarged Potential Window. *Electrochim. Acta* **2012**, *74*, 65–72.
39. He, L.; Ma, R.; Du, N.; Ren, J.; Wong, T.; Li, Y.; Lee, T. S. Growth of TiO_2 Nanorod Arrays on Reduced Graphene Oxide with Enhanced Lithium-Ion Storage. *J. Mater. Chem.* **2012**, *22*, 19601–19066.
40. Cao, H.; Li, B.; Zhang, J.; Lian, F.; Kong, X.; Qu, M. Synthesis and Superior Anode Performance of TiO_2@Reduced Graphene Oxide Nanocomposites for Lithium Ion Batteries. *J. Mater. Chem.* **2012**, *22*, 9759–9766.
41. Wen, W. J.; Huang, X. X.; Yang, S. H.; Lu, K. Q.; Sheng, P. The Giant Electrorheological Effect in Suspensions of Nanoparticles. *Nat. Mater.* **2003**, *2*, 727–730.
42. Fang, T. T.; Lin, H. B.; Hwang, J. B. Thermal-Analysis of Precursors of Barium-Titanate Prepared by Coprecipitation. *J. Am. Ceram. Soc.* **1990**, *73*, 3363–3367.
43. Chen, J. S.; Liu, H.; Qiao, S. Z.; Lou, X. W. Carbon-Supported Ultrathin Anatase TiO_2 Nanosheets for Fast Reversible Lithium Storage. *J. Mater. Chem.* **2011**, *21*, 5687–5692.
44. Lindstrom, H.; Sodergren, S.; Solbrand, A.; Rensmo, H.; Hjelm, J.; Hagfeldt, A.; Lindquist, S. E. Li^+ Ion Insertion in TiO_2 (Anatase). 2. Voltammetry on Nanoporous Films. *J. Phys. Chem. B* **1997**, *101*, 7717–7722.
45. Maier, J. Nanoionics: Ion Transport and Electrochemical Storage in Confined Systems. *Nat. Mater.* **2005**, *4*, 805–815.
46. Zhukovskii, Y. F.; Balaya, P.; Kotomin, E. A.; Maier, J. Evidence for Interfacial-Storage Anomaly in Nanocomposites for Lithium Batteries from First-Principles Simulations. *Phys. Rev. Lett.* **2006**, *96*, 058302.
47. Shin, J.-Y.; Samuelis, D.; Maier, J. Sustained Lithium-Storage Performance of Hierarchical, Nanoporous Anatase TiO_2 at High Rates: Emphasis on Interfacial Storage Phenomena. *Adv. Funct. Mater.* **2011**, *21*, 3464–3472.
48. Yang, H.; Wu, X.-L.; Cao, M.-H.; Guo, Y.-G. Solvothermal Synthesis of $LiFePO_4$ Hierarchically Dumbbell-Like Microstructures by Nanoplate Self-Assembly and Their Application as a Cathode Material in Lithium-Ion Batteries. *J. Phys. Chem. C* **2009**, *113*, 3345–3351.

49. Luo, J.-Y.; Xiong, H.-M.; Xia, Y.-Y. $LiMn_2O_4$ Nanorods, Nanothorn Microspheres, and Hollow Nanospheres as Enhanced Cathode Materials of Lithium Ion Battery. *J. Phys. Chem. C* **2008**, *112*, 12051–12057.
50. Wu, Z.-S.; Ren, W.; Xu, L.; Li, F.; Cheng, H.-M. Doped Graphene Sheets As Anode Materials with Superhigh Rate and Large Capacity for Lithium Ion Batteries. *ACS Nano* **2011**, *5*, 5463–5471.
51. Pan, D.; Wang, S.; Zhao, B.; Wu, M.; Zhang, H.; Wang, Y.; Jiao, Z. Li Storage Properties of Disordered Graphene Nanosheets. *Chem. Mater.* **2009**, *21*, 3136–3142.
52. Wang, H. E.; Lu, Z. G.; Xi, L. J.; Ma, R. G.; Wang, C. D.; Zapien, J. A.; Bello, I. Facile and Rapid Synthesis of Highly Porous Wirelike TiO_2 as Anodes for Lithium-Ion Batteries. *ACS Appl. Mater. Inter.* **2012**, *4*, 1608–1613.
53. Zhou, X.; Liu, Z. A Scalable, Solution-Phase Processing Route to Graphene Oxide and Graphene Ultralarge Sheets. *Chem.Commun.* **2010**, *46*, 2611–2613.